

A neuroprotective role for microglia in prion diseases

Caihong Zhu,* Uli S. Herrmann,* Jeppe Falsig, Irina Abakumova, Mario Nuvolone, Petra Schwarz, Katrin Frauenknecht, Elisabeth J. Rushing, and Adriano Aguzzi

Institute of Neuropathology, University Hospital Zurich, 8091 Zurich, Switzerland

Microglial activation is a hallmark of most neurodegenerative disorders, and is particularly conspicuous in prion diseases. However, the role of microglia, which function as both primary immune effector cells and professional phagocytes in the central nervous system, remains contentious in the context of neurodegeneration. Here, we evaluated the effect of microglial depletion/deficiency on prion pathogenesis. We found that ganciclovir-mediated microglial ablation on *tga20/CD11b*-thymidine kinase of Herpes simplex virus (HSVTK) cerebellar organotypic cultured slices markedly aggravated prion-induced neurotoxicity. A similar deterioration of disease was recapitulated in in vivo microglial depletion in prion-infected *tga20/CD11b*-HSVTK mice. Additionally, deficiency of microglia in interleukin 34 knockout (*IL34*^{-/-}) mice again resulted in significantly augmented proteinase K-resistant prion protein deposition and accelerated prion disease progression. These results provide unambiguous evidence for a general protective role of microglia in prion pathogenesis.

Microglia are the primary immune cells in the CNS, arising from c-kit⁺ erythromyeloid precursors in the yolk sac, and then migrating to the developing neural tube to mature (Alliot et al., 1999; Ginhoux et al., 2010; Schulz et al., 2012; Kierdorf et al., 2013). In the brain, microglia interact with neurons and exert a wide variety of physiological functions (Chen et al., 2010; Paolicelli et al., 2011; Rogers et al., 2011; Derecki et al., 2012; Schafer et al., 2012; Parkhurst et al., 2013; Zhan et al., 2014). As an integral part of the innate immune system, microglia constantly patrol the brain parenchyma and subsequently clear pathogens, apoptotic cells, and cellular debris by phagocytosis under physiological and pathological conditions (Davalos et al., 2005; Nimmerjahn et al., 2005; Mildner et al., 2011). However, microglia can be activated by various triggering factors, such as injury, infection, or neurodegeneration, leading to morphological and molecular changes and release of cytokines (Aguzzi et al., 2013a). Depending on the type of molecular stimuli and cues received from the surrounding microenvironment, microglia can take on many different activation profiles and are thought to exert both beneficial and detrimental effects (Hanisch and Kettenmann, 2007).

Prion diseases are progressive neurodegenerative disorders associated with striking microglial activation (Aguzzi et al., 2013b). In animal models of prion disease, microglial activation and cytokine release occur at an early stage of the disease and are found in areas of proteinase K (PK)-resistant prion protein (PrP^{Sc}) deposition, but precede spongiosis

and neuronal loss (Williams et al., 1997; Giese et al., 1998). As in other protein misfolding diseases, microglia are found surrounding PrP^{Sc} plaques and intracellular PrP^{Sc} can be detected in microglia (Jeffrey et al., 1994; Baker et al., 2002). The presence of high prion infectivity in microglia suggests that microglia may disseminate prions within the CNS (Baker et al., 2002). In addition, the cytokines produced by activated microglia may contribute to progression of the disease.

In contrast, microglia are also professional phagocytes in the brain and can engulf and degrade PrP^{Sc}. Indeed, microglial depletion from CD11b-thymidine kinase of Herpes simplex virus (HSVTK) cerebellar organotypic cultured slices (COCS) infected with RML6 prions (Rocky Mountain Laboratories, scrapie strain passage #6) results in increased deposition of PrP^{Sc} and augmented prion titers, indicating that microglia play an important role in the clearance of prions (Falsig and Aguzzi, 2008; Falsig et al., 2008). Nevertheless, because of the dearth of appropriate animal models, the exact role of microglia in prion pathogenesis remains unknown.

In this study, we first assessed the role of microglia in prion pathogenesis using pharmacogenetic microglia depletion ex vivo and in vivo (Heppner et al., 2005). We found that microglia ablation drastically enhanced the neurotoxicity of prions ex vivo and shortened the lifespan of prion-infected mice. We also administered prions to IL-34-ablated (*IL34*^{-/-}) mice, which have a reduced number of microglia (Greter et al., 2012; Wang et al., 2012). We found enhanced PrP^{Sc} deposition and accelerated prion progression compared with WT littermates. These results indicate that microglia play an overall protective rather than deleterious role in prion disease.

*C. Zhu and U.S. Herrmann contributed equally to this paper.

Correspondence to Adriano Aguzzi: Adriano.Aguzzi@usz.ch; or Caihong Zhu: Caihong.Zhu@usz.ch

Abbreviations used: CGN, cerebellar granule neuron; COCS, cerebellar organotypic cultured slices; dpi, days postinoculation; GCV, ganciclovir; HSVTK, thymidine kinase of Herpes simplex virus; NBH, noninfectious brain homogenate; PK, proteinase K; PLC, peritoneal lavage cell; PrP^{Sc}, PK-resistant prion protein; qRT-PCR, quantitative real-time PCR; RML6, Rocky Mountain Laboratories scrapie, strain passage #6.

© 2016 Zhu et al. This article is distributed under the terms of an Attribution-Noncommercial-Share Alike-No Mirror Sites license for the first six months after the publication date (see <http://www.rupress.org/terms>). After six months it is available under a Creative Commons License (Attribution-Noncommercial-Share Alike 3.0 Unported license, as described at <http://creativecommons.org/licenses/by-nc-sa/3.0/>).

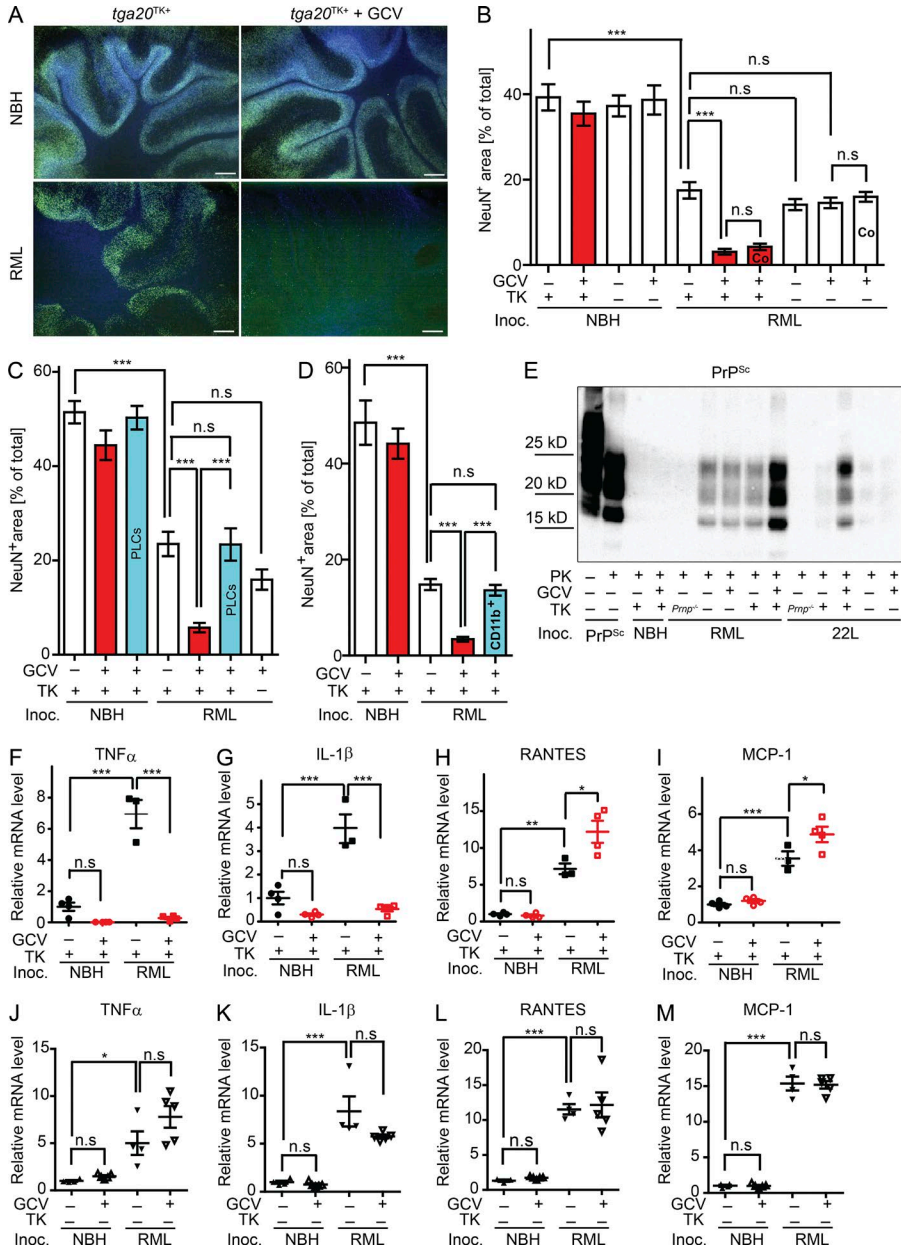


Figure 1. Microglia ablation on CD11b-HSVTK COCS enhanced prion-induced neurotoxicity. (A and B) *tga20^{TK+}* or *tga20^{TK-}* slices were treated with NBH or RML6 and cultured in the optional presence of GCV for 49 dpi. Representative COCS stained for NeuN (green) and DAPI (blue); (A) and analyzed by NeuN morphometry (B). Bars, 200 μ m. *n* = 10–11. ***, *P* < 0.001; *n.s.*, *P* > 0.05. Bars labeled Co denote co-culture of slices divided by a grease barrier. Red bars indicate microglia depletion. (C) NeuN morphometry of RML6 infected *tga20^{TK+}* COCS optionally treated with GCV and reconstituted with PLCs prepared from *tga20* mice (~70,000 cells per COCS). Red: microglia-depleted, Blue: microglia-depleted and PLC reconstituted. *n* = 10; ***, *P* < 0.001; *n.s.*, *P* > 0.05. (D) NeuN morphometry of RML6 infected *tga20^{TK+}* COCS optionally treated with GCV and reconstituted with 70×10^3 CD19⁺CD11b⁺ cells per slice. Red: microglia-depleted, Blue: microglia-depleted and CD19⁺CD11b⁺ cells reconstituted. *n* = 10. ***, *P* < 0.001. (E) PrP^{Sc} Western blot of cultures prepared from *Prnp^{-/-}*, *tga20^{TK+}*, or *tga20^{TK-}* mice exposed to NBH, RML6, or 22L and cultured until 35 dpi in the optional presence of GCV. Samples were digested with PK as indicated and detected with POM1. (F–I) qRT-PCR of cytokines and chemokines in *tga20^{TK+}* slices treated with NBH or RML6 at 42 dpi \pm GCV. (J–M) qRT-PCR of cytokines and chemokines in *tga20^{TK-}* slices treated with NBH or RML6 at 42 dpi \pm GCV. (F and J) TNF mRNA, (G and K) IL-1 β mRNA, (H and L) RANTES mRNA, and (I and M) MCP-1 mRNA. *n* = 3–5. *, *P* < 0.05; **, *P* < 0.01; ***, *P* < 0.001; *n.s.*, *P* > 0.05. Relative expression normalized to GAPDH expression and represented as fold change compared with noninfected, non-GCV samples \pm SEM. Statistical significance in B–D and F–M was determined using one-way ANOVA with Tukey's post-test for multicolumn comparison. Histology, Western blot, and qRT-PCR results represent at least three independent experiments.

RESULTS

Microglial ablation increases the neurotoxicity of prions in the ex vivo CD11b-HSVTK system

Prion pathogenesis is faithfully reproduced in the COCS system (Falsig et al., 2012; Herrmann et al., 2015). Hence, we evaluated the role of microglia in COCS prepared from *tga20*:CD11b-HSVTK mice (*tga20^{TK+}*), which were obtained by intercrossing mice overexpressing the cellular prion protein PrP^C (Fischer et al., 1996) and mice expressing the HSV TK under the control of the CD11b promoter (Heppner et al., 2005). Administration of ganciclovir (GCV) to *tga20^{TK+}* COCS leads to complete microglial ablation after 14 d of treatment (Falsig et al., 2008). Therefore, *tga20^{TK+}* COCS

were exposed to RML6 or noninfectious brain homogenate (NBH), and GCV-mediated microglial ablation was performed. At 49 d postinoculation (dpi), RML6-infected non-GCV-treated *tga20^{TK+}* COCS showed a significant decrease in the density of NeuN⁺ cerebellar granule neurons (CGN) compared with NBH-treated *tga20^{TK+}* COCS (Fig. 1, A and B). However, depletion of microglia (RML6-infected, GCV-treated *tga20^{TK+}* COCS) resulted in a dramatic increase in neurotoxicity, leading to subtotal CGN depletion in COCS (Fig. 1, A and B). Therefore, GCV treatment significantly increased neurotoxicity in RML6-infected *tga20^{TK+}* cultures compared with RML6-infected, non-GCV-treated *tga20^{TK+}* COCS.

The exacerbation of neurotoxicity may be a result of GCV-mediated microglial ablation or of direct toxicity of GCV to COCS. To discriminate between these possibilities, NBH-exposed *tga20^{TK+}* COCS were treated with GCV. The viability of NeuN⁺ CGN was similar to that of NBH-exposed non-GCV-treated *tga20^{TK+}* COCS (Fig. 1 B). Additionally, GCV treatment of RML6-infected *tga20^{TK-}* COCS had no effect on neurotoxicity (Fig. 1 B). These results indicate that microglia are not essential for the long-term survival of COCS, but play a protective role in prion pathogenesis in COCS.

We then asked if phosphorylated GCV released from dying microglia might affect the viability of bystander neurons in the context of prion infection. We co-cultured prion-infected *tga20^{TK+}* and *tga20^{TK-}* slices in the presence of GCV. Cultures were separated by a grease barrier to prevent microglia migration from TK⁻ to TK⁺ cultures but allowing for the exchange of solutes, including GCV and its metabolites. GCV-treated *tga20^{TK-}* slices co-cultured with *tga20^{TK+}* slices developed pathology similarly to GCV-treated *tga20^{TK-}* slices cultured separately (Fig. 1 B). Hence, we failed to detect any evidence that dying microglia in *tga20^{TK+}* slices release soluble neurotoxic factors. Similarly, co-cultured GCV-treated *tga20^{TK+}* slices showed an equivalent pathology to GCV-treated *tga20^{TK+}* slices cultured separately (Fig. 1 B), suggesting that microglia in *tga20^{TK-}* slices did not release soluble neuroprotective factors into the medium.

We previously found that microglia-depleted COCS can be reconstituted with peritoneal lavage cells (PLCs), and that this decreases PrP^{Sc} accumulation (Falsig et al., 2008). Reconstitution of prion-infected microglia-depleted *tga20^{TK+}* slices with *tga20* PLCs (70,000 cells/COCS) completely repressed the increased toxicity in GCV-treated COCS (Fig. 1 C).

Furthermore, we used magnetic cell sorting (MACS) to purify CD11b⁺ cells from PLCs. Using this procedure, we achieved a 96.4% purity of the CD11b⁺ fraction, whereas the unsorted PLCs contained only 60.9% CD11b⁺ cells. Prion-infected, microglia-depleted GCV-treated *tga20^{TK+}* cultures were reconstituted with purified CD11b⁺ cells, and the degrees of reconstitution and cell death were assessed at 49 dpi. Again, reconstitution of RML6-infected *tga20* COCS with CD11b⁺ PLCs restored the neuroprotection that had been abolished by GCV treatment (Fig. 1 D). The variability in NeuN values (Fig. 1, B–D) results from intrinsic variations in primary slice viability.

As previously reported (Falsig et al., 2008), microglial ablation leads to increased accumulation of PrP^{Sc} in COCS infected not only by RML6 but also by 22L, whereas non-GCV-treated and GCV-treated *tga20^{TK-}* COCS show similar accumulation of PrP^{Sc} (Fig. 1 E). In addition, prion infection up-regulated the expression of proinflammatory markers, including cytokines (TNF and IL-1 β) and chemokines (MCP-1 and RANTES) in COCS at late time points (42 dpi; Falsig et al., 2012). In prion-infected *tga20^{TK+}* COCS (42 dpi), TNF, IL1 β , RANTES, and MCP-1 were up-regulated

(Fig. 1, F–I), but microglial depletion only abolished the expression of TNF and IL-1 β in prion-infected COCS (Fig. 1, F and G), whereas up-regulation of RANTES and MCP-1 was accentuated after microglia depletion (Fig. 1, H and I). In *tga20^{TK-}* COCS, the up-regulation of TNF, IL-1 β , RANTES and MCP-1 upon RML6 infection was not affected by GCV treatment (Fig. 1, J–M). Hence, microglia-depleted tissue accumulates more PrP^{Sc} but does not up-regulate TNF and IL-1 β . Notwithstanding the significant reduction of proinflammatory cytokines (TNF and IL-1 β), microglial ablation still enhanced prion pathogenesis, suggesting that microglia play a protective role in prion pathogenesis in COCS and activated microglia-derived cytokines are not important contributors to prion disease (Aguzzi et al., 2013b).

Microglial ablation increases the neurotoxicity of prions in the in vivo CD11b-HSVTK system

Intraventricular administration of GCV to CD11b-HSVTK mice using osmotic minipumps efficiently depletes microglia in vivo (Grathwohl et al., 2009). Because microglia-depleted mice die after ~4 wk of GCV administration, possibly because of intracerebral hemorrhages (Grathwohl et al., 2009), we intercrossed CD11b-HSVTK mice and *tga20* mice to obtain a homozygous *tga20* transgene (*tga20^{+/+;TK+}*) and to enable microglial depletion in an accelerated prion disease model (Fischer et al., 1996). We inoculated *tga20^{+/+;TK+}* and *tga20^{+/+;TK-}* mice with RML6 or NBH intracerebrally. At 38 dpi, we implanted osmotic minipumps loaded with GCV (microglia depletion) or PBS (for control) that delivered the compounds into the ventricle. RML6-infected *tga20^{+/+;TK-}* mice treated with PBS or GCV and *tga20^{+/+;TK+}* mice treated with PBS developed terminal scrapie with median incubation times of 56–57 dpi (Fig. 2 A). In contrast, *tga20^{+/+;TK+}* mice treated with GCV showed a median incubation time of 50 dpi, with a highly significant acceleration of progression compared with PBS-treated *tga20^{+/+;TK+}* mice (7 d; $P < 0.0001$; Fig. 2 A); under no other conditions were *tga20* mice reported to develop scrapie so rapidly. Life span reduction was caused by neither microglia depletion alone nor by the surgical implantation of osmotic pump; PBS-treated *tga20^{+/+;TK+}* mice inoculated with NBH survived up to 100 d postimplantation (138 dpi) and GCV-treated *tga20^{+/+;TK+}* mice inoculated with NBH died at 24 d postimplantation, whereas RML6-infected GCV-treated *tga20^{+/+;TK+}* mice became terminally sick at 12 d postimplantation (Fig. 2 A).

RML6-infected *tga20^{+/+;TK+}* mice treated with GCV showed a marked depletion of microglia in the cortex (82% reduction), compared with RML6-infected PBS treated *tga20^{+/+;TK+}* or GCV-treated *tga20^{+/+;TK-}* mice (Fig. 2, B and C). Noninfected *tga20^{+/+;TK+}* mice showed a slightly less efficient microglia depletion (63% reduction), suggesting that prion infection enhanced GCV-mediated microglia depletion (Fig. 2 C). Similarly, microglia depletion was observed in the cerebellum, showing that widespread microglia depletion was efficiently attained (Fig. 2 D). In agreement with previous

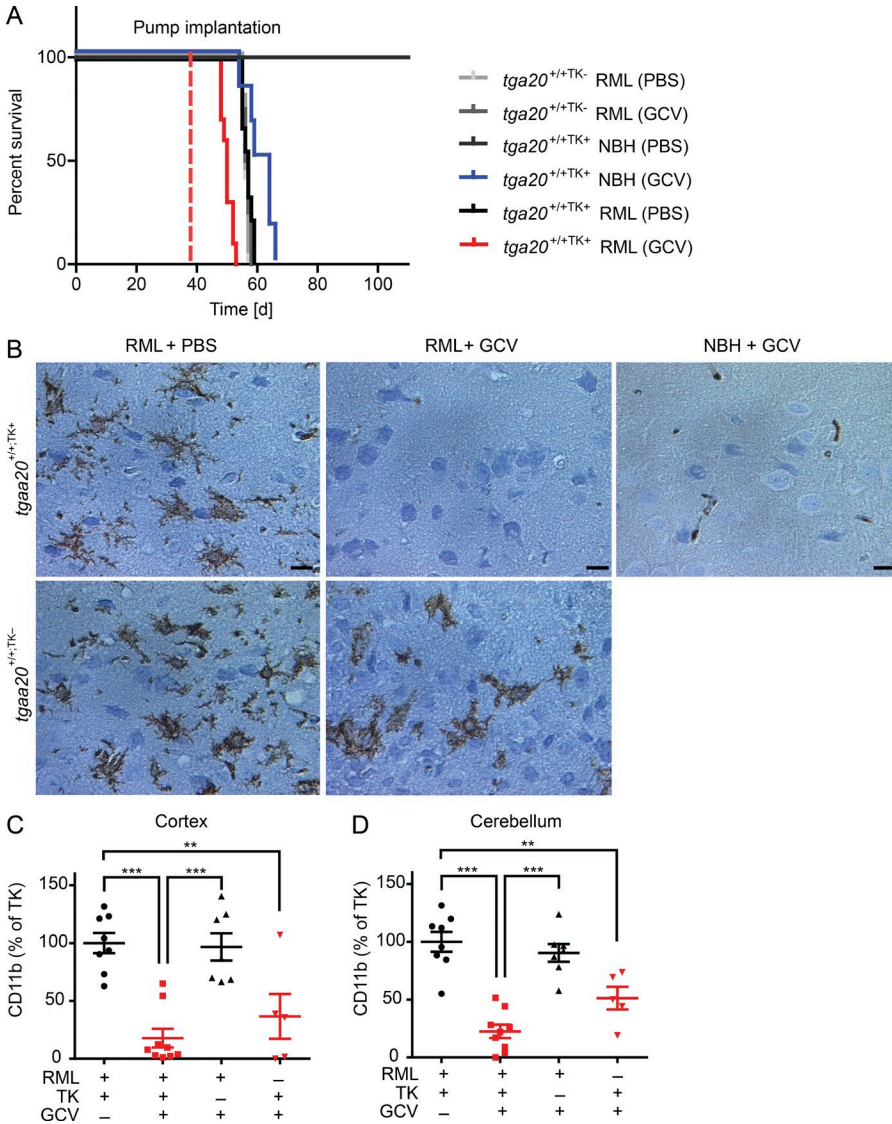


Figure 2. Microglia ablation on in vivo CD11b-HSVTK system deteriorated prion disease. (A) Survival curves of RML6- or NBH-inoculated *tga20*^{+/+TK+} or *tga20*^{+/+TK-} mice implanted with GCV or PBS containing intra-ventricular osmotic minipumps (*tga20*^{+/+TK-} RML(PBS), *n* = 5, median survival = 56 dpi; *tga20*^{+/+TK-} RML(GCV), *n* = 4, median survival = 56.5 dpi; *tga20*^{+/+TK+} NBH(PBS), *n* = 6, remained asymptomatic up to 138 dpi; *tga20*^{+/+TK+} NBH(GCV), *n* = 6, median survival = 61.5 dpi; *tga20*^{+/+TK+} RML(PBS), *n* = 9, median survival = 57 dpi; *tga20*^{+/+TK+} RML(GCV), *n* = 10, median survival = 50 dpi; ****, *P* < 0.0001). Dashed line represents time of pump implantation. Microglia-depleted mice showed an accelerated prion progression as compared with all other groups. (B) Iba1 immunohistochemistry of cortical brain tissue from all experimental groups showing dramatic reduction in the microglial colonization of GCV-treated, RML6-infected *tga20*^{+/+TK+} mice. Bars, 10 μm. (C and D) Quantification of microglia depletion in (C) cortical (*tga20*^{+/+TK+} RML(PBS), *n* = 8; *tga20*^{+/+TK+} RML(GCV), *n* = 9; *tga20*^{+/+TK-} RML(GCV), *n* = 7; *tga20*^{+/+TK+} NBH(GCV), *n* = 5; **, *P* < 0.01; ***, *P* < 0.001) or (D) cerebellar tissue (*tga20*^{+/+TK+} RML(PBS), *n* = 8; *tga20*^{+/+TK+} RML(GCV), *n* = 9; *tga20*^{+/+TK-} RML(GCV), *n* = 8; *tga20*^{+/+TK+} NBH(GCV), *n* = 5; ***, *P* < 0.001; **, *P* < 0.01). Red, microglia depleted. Error bars represent SEM. Statistical significance in A was determined using Log-rank (Mantel-Cox) test. Statistical significance in C and D was determined using one-way ANOVA with Tukey's post-test for multicolumn comparison. Histology results represent at least five independent experiments.

studies (Grathwohl et al., 2009), we did not observe aplastic anemia as a result of GCV delivery directly to the brain of HSVTK-expressing mice (Fig. S1).

Accelerated prion pathogenesis in microglia-deficient *IL34*^{-/-} mice

To further validate the protective role of microglia in prion pathogenesis, *IL34*^{-/-} mice that contain a reduced number of microglia (Wang et al., 2012), but express a similar amount of PrP^C as WT mice (Fig. 3, A and B), were intracerebrally inoculated with RML6 prions. Mice were monitored for clinical signs of scrapie. The incubation time was defined as the time lag between prion inoculation and the time at which mice were euthanized, which corresponded to the terminal stage of prion disease. We found that both female and male *IL34*^{-/-} mice showed significantly accelerated prion progression when compared with age- and gender-matched WT littermates

(median survival 162 dpi for female *IL34*^{-/-} vs. 176 dpi for female *IL34*^{+/+}, *P* = 0.0025; median survival 170 dpi for male *IL34*^{-/-} vs. 191 dpi for male *IL34*^{+/+}, *P* < 0.0001; Fig. 3 C).

To address whether the accelerated prion progression in *IL34*^{-/-} mice resulted from the deficiency of microglia and impaired PrP^{Sc} clearance, we compared PrP^{Sc} levels at a presymptomatic and at a clinically overt stage (105 dpi at ~5 mo of age and 150 dpi at ~7.5 mo of age, respectively). Clinically sick mice showed a characteristic scrapie phenotype with waddling gait, mildly reduced grooming, and initial paresis. We observed significantly more PrP^{Sc} deposition in *IL34*^{-/-} brains, suggesting that microglia play a protective role in prion pathogenesis by, at least partially, clearing PrP^{Sc} in the brain (Fig. 3, D–G).

Surprisingly, the density of microglia did not differ between *IL34*^{-/-} and their WT littermates at 105 dpi and 150 dpi (Fig. 4, A–D). Because *IL-34*^{-/-} mice contain less mi-

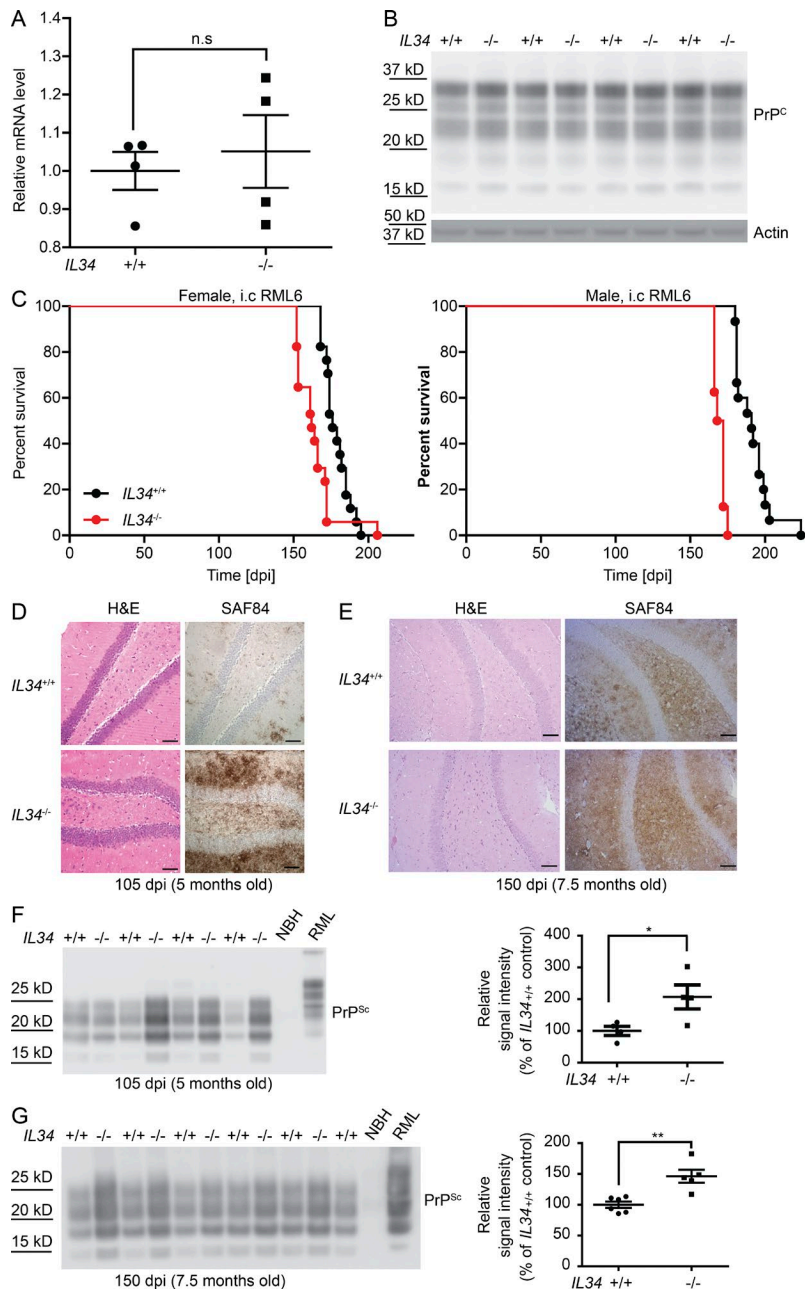


Figure 3. Microglia-deficient *IL34*^{-/-} mice demonstrated accelerated prion pathogenesis. (A) qRT-PCR for *Prnp* mRNA in one hemisphere of *IL34*^{-/-} and *IL34*^{+/+} brains. *n* = 4. n.s., *P* > 0.05. (B) PrP^{Sc} Western blot for one hemisphere from *IL34*^{-/-} and *IL34*^{+/+} brains. *n* = 4. (C) Survival curves of RML6 infected *IL34*^{-/-} and *IL34*^{+/+} (WT) mice. Median survival of *IL34*^{-/-} females 162 dpi (*n* = 17) versus *IL34*^{+/+} (WT) females 176 dpi (*n* = 17). **, *P* < 0.01; median survival of *IL34*^{-/-} males 170 dpi (*n* = 8) versus *IL34*^{+/+} (WT) males 191 dpi (*n* = 15). ****, *P* < 0.0001. (D and E) Hematoxylin and eosin and SAF84 staining on RML6-infected *IL34*^{-/-} and *IL34*^{+/+} (WT) brains at 105 dpi (D) and 150 dpi (E). Bars, 50 μm. (F and G, left) PrP^{Sc} Western blot of homogenates prepared from one brain hemisphere of RML6-infected *IL34*^{-/-} and *IL34*^{+/+} (WT) mice at 105 dpi (F) and 150 dpi (G). Samples were digested with PK as indicated and detected with POM1. (right) Densitometric quantification of the PrP^{Sc} Western blot. *n* = 4 (105 dpi) or 5 (150 dpi) for *IL34*^{-/-}; *n* = 4 (105 dpi) or 6 (150 dpi) for *IL34*^{+/+}. **, *P* < 0.01; *, *P* < 0.05. Error bars represent SEM. Survival curves summarize two independent i.c. inoculation experiments. Statistical significance in A, F, and G was determined using unpaired Student's *t* test. Statistical significance in C and D was determined using Log-rank (Mantel-Cox) test. qRT-PCR, histology, and Western blot results represent at least four independent experiments.

croglia under physiological conditions (Greter et al., 2012; Wang et al., 2012), this finding suggests that the proliferative stimulus exerted by prion infection can partially compensate for the lack of IL-34. However, in this situation, microglia may be less effective at clearing PrP^{Sc} (Hughes et al., 2010; Gómez-Nicola et al., 2013).

Cytokine profiling was also performed and no significant difference was observed between these two groups, indicating that IL-34 is not involved in prion-induced cytokine expression (Fig. 4, E–J). On the contrary, we observed significantly more astrogliosis (GFAP immunoreactivity) in *IL34*^{-/-} brains (Fig. 4, K–N), probably as a result of enhanced

PrP^{Sc} accumulation. In terminally sick *IL34*^{-/-} (~8-mo-old) and WT (~8.5-mo-old) littermates, which showed scrapie symptoms including ataxia, paresis, and reduced activity, no obvious difference in PrP^{Sc} deposition (Fig. 5, A and B), microglial activation (Fig. 5, C and D), or astrogliosis was observed (Fig. 5, E–F). In summary, in the microglia deficiency *IL34*^{-/-} mouse model we confirmed that microglia play an overall protective role in prion pathogenesis.

DISCUSSION

Neuroinflammation is a term that was originally coined to denote lymphocytic and purulent CNS infiltrates that

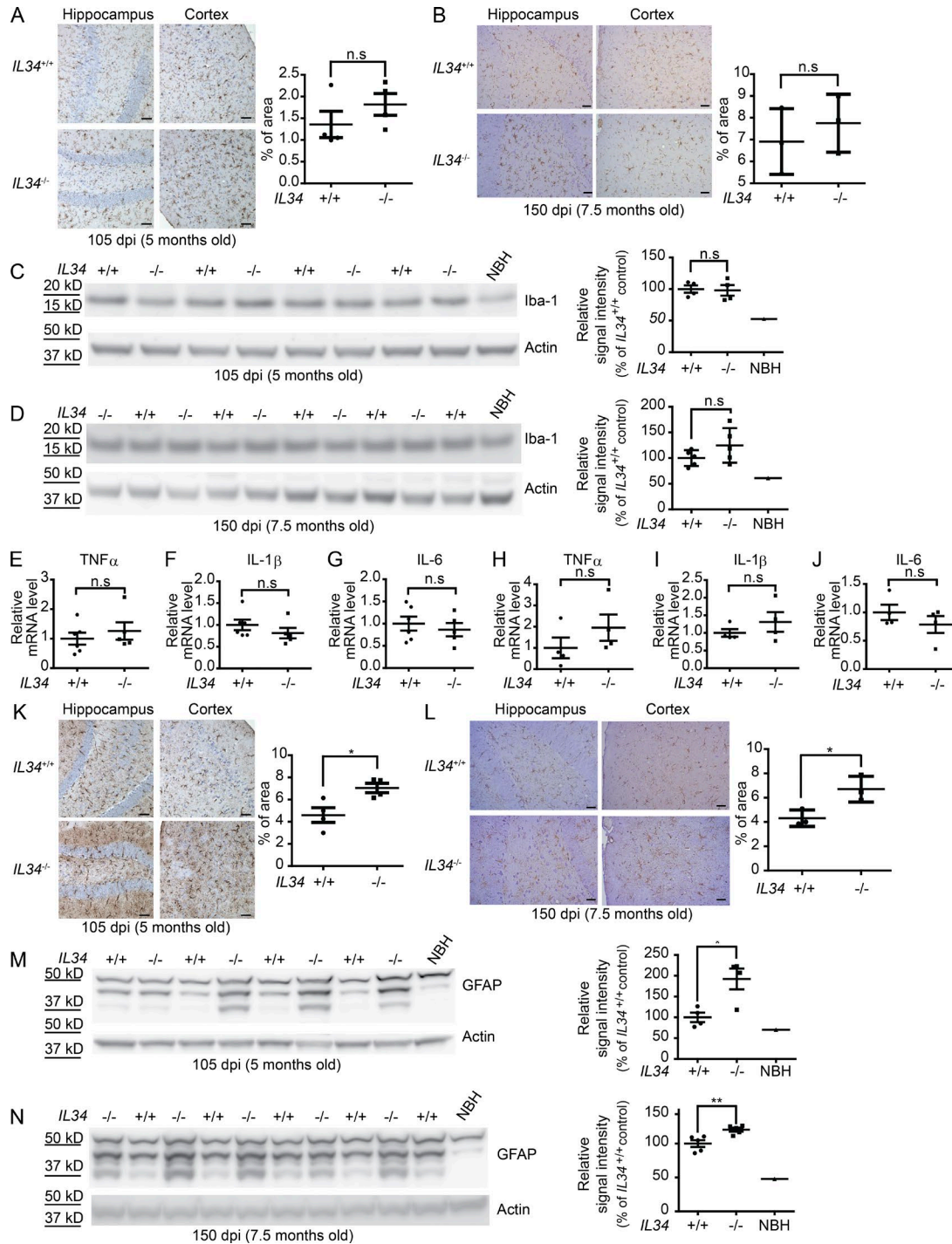


Figure 4. **Microglia-deficient *IL34*^{-/-} mice displayed similar microglial activation, but augmented astrogliosis.** (A, left) Iba1 immunohistochemistry of brain tissues from RML6-infected *IL34*^{-/-} and *IL34*^{+/+} (WT) mice at 105 dpi. (right) Quantification of the Iba1 immunostaining. *n* = 4; n.s, *P* > 0.05. Bars, 20 μ m. (B, left) Iba1 immunohistochemistry of brain tissues from RML6-infected *IL34*^{-/-} and *IL34*^{+/+} (WT) mice at 150 dpi. (right) Quantification of the Iba1 immunostaining. *n* = 3; n.s, *P* > 0.05. Bars, 20 μ m. (C, left) Iba1 Western blot of one hemisphere from RML6-infected *IL34*^{-/-} and *IL34*^{+/+} (WT) mice at 105 dpi. (right) Densitometric quantification of the Iba1 Western blot. *n* = 4; n.s, *P* > 0.05. (D, left) Iba1 Western blot of one hemisphere from RML6-infected *IL34*^{-/-} and *IL34*^{+/+} (WT) mice at 150 dpi. (right) Densitometric quantification of the Iba1 Western blot. *n* = 5; n.s, *P* > 0.05. (E–J) qRT-PCR of cytokines from one hemisphere of RML6-infected *IL34*^{-/-} and *IL34*^{+/+} (WT) mice at 105 dpi (E–G) and 150 dpi (H–J). (E and H) TNF mRNA, (F and I) IL-1 β mRNA, and (G and J) IL-6 mRNA. Relative expression normalized to GAPDH expression and represented as fold change compared with WT mice \pm SEM. *n* = 4 (105 dpi) or 5 (150 dpi) for *IL34*^{-/-}; *n* = 4 (105 dpi) or 6 (150 dpi) for *IL34*^{+/+}, n.s, *P* > 0.05. (K, left) GFAP immunohistochemistry of brain tissues from RML6-infected *IL34*^{-/-} and

accompany infections and autoimmune diseases. More recently, however, the term has been expanded to include microglial activation typically encountered in neurodegenerative diseases that do not have a primary inflammatory pathogenesis, such as Alzheimer's disease, Parkinson's disease, and prion disease (Aguzzi and Falsig, 2012). The contribution of microglial activation to the pathogenesis of these diseases has emerged as a central question and may encompass both beneficial and detrimental aspects. Microglia are immune cells, which respond to various stimuli that trigger the release of proinflammatory factors that could potentially damage the brain. However, microglia are professional phagocytes that engulf and degrade pathogens and apoptotic bodies, and therefore also exert protective and defensive functions in the CNS. The overall role of microglia in neurodegeneration is likely to depend on environmental cues, many of which remain undeciphered, which can turn microglia into either friends or foes in disparate conditions.

Among the neurodegenerative disorders, prion diseases are associated with the most dramatic microglial activation. Although a role for microglia in prion diseases was implicated in a study using prion protein–derived peptide PrP^{106–126} (Brown et al., 1996), that peptide has never been detected in vivo and is not infectious per se, which raises serious doubts about the validity of those findings. Another study demonstrated that blocking microglial proliferation with a CSF1R inhibitor could slow neuronal damage and disease progression (Gómez-Nicola et al., 2013), suggesting a harmful contribution of microglia to prion disease. However, the overall role of microglia in prion diseases has remained unclear, largely because of the lack of an appropriate mouse model.

Here, we reasoned that the aforementioned question might be best studied by using several model systems that modify microglial functions in independent ways. Because organotypic CD11b-HSVTK COCS allow for the most radical—yet exquisitely specific—ablation of microglia, we opted to investigate prion pathogenesis in this system. We previously reported that microglial ablation from short-term COCS unleashes prion replication (Falsig et al., 2008), but at that time we had not yet discovered that prion infection leads to neurodegeneration in long-term COCS. Consequently, we had been unable to investigate whether microglia ablation would affect neurodegeneration, either positively or negatively. The improved COCS culture system used here allowed us to address the latter question. Not only did we confirm our previous study that depletion of microglia in COCS leads to enhanced PrP^{Sc} deposition, but we also detected a dra-

matic acceleration in prion-induced neurodegeneration of the cerebellar granule layer. Notably, microglia ablation does not affect antiprion antibody-induced neurotoxicity (Sonati et al., 2013), suggesting that microglia exert neuroprotection by reducing the prion load rather than by acting on downstream events shared by prion infections and antiprion antibody treatment (Herrmann et al., 2015).

The notion that microglia protects the brain against prion-induced neurotoxicity was confirmed in vivo using CD11b-HSVTK transgenic mice. This model results in drastic microglia reduction, yet it suffers from limitations in the observational time span. Because the CD11b transgene is ectopically expressed in hematopoietic stem cells, administration of GCV to CD11b-HSVTK⁺ transgenic mice leads to aplastic anemia and hemorrhagic diathesis. This issue can be alleviated (but not eliminated) by administering smaller doses of GCV intracerebrally through osmotic minipumps, thereby minimizing systemic exposure to the drug. These limitations forced us to devise a particularly rapid model of prion disease, i.e., the inoculation of mice carrying homozygous arrays of the *tga20* transgene. Although this experimental design exaggerates certain aspects of prion pathology, the salient characteristics of the disease (including spongiform encephalopathy, astrogliosis, and PrP^{Sc} deposition) are faithfully reproduced, and we found that microglial depletion has a major deleterious effect on prion-induced neurodegeneration.

We then wondered whether the conclusions drawn from the aforementioned studies would be verifiable in a system in which microglia are compromised. Toward that goal, we used *IL34*^{-/-} mice that suffer from impaired microglial development or maintenance and reduced microglia numbers (Greter et al., 2012; Wang et al., 2012). We again observed microglial deficiency resulting in accelerated prion progression and enhanced PrP^{Sc} deposition. All of these results suggest that microglia play an overall protective role in prion pathogenesis.

Interestingly, although microglia numbers were reduced in *IL34*^{-/-} mice, upon prion infection microglia reached numbers similar to WT littermates. We conclude that IL-34 is not required for prion-induced microglial activation and proliferation. The increased deposition of PrP^{Sc} and accelerated prion disease in *IL34*^{-/-} brains may therefore be caused by the scarcity of microglia at early stages of prion infection, or alternatively, to poorly understood defects in the effector functions of microglia.

IL-34^{-/-} mice exhibited more astrogliosis than WT mice at 105 and 150 dpi, probably as a consequence of enhanced PrP^{Sc} deposition. Alternatively, astrogliosis may conceivably

IL34^{+/+} (WT) mice at 105 dpi. (right) Quantification of the GFAP immunostaining, $n = 4$, *, $P < 0.05$. Bars, 20 μm . (L, left) GFAP immunohistochemistry of brain tissues from RML6-infected *IL34*^{-/-} and *IL34*^{+/+} (WT) mice at 150 dpi. (right) Quantification of the GFAP immunostaining, $n = 3$; *, $P < 0.05$. Bars, 20 μm . (M, left) GFAP Western blot of one hemisphere from RML6-infected *IL34*^{-/-} and *IL34*^{+/+} (WT) mice at 105 dpi. (right) Densitometric quantification of the GFAP Western blot. $n = 4$ for *IL34*^{-/-}; $n = 4$ for *IL34*^{+/+}; *, $P < 0.05$. (N, left) GFAP Western blot of one hemisphere from RML6-infected *IL34*^{-/-} and *IL34*^{+/+} (WT) mice at 150 dpi. (right) Densitometric quantification of the GFAP Western blot. $n = 5$, **, $P < 0.01$. Error bars represent SEM. Statistical significance in A–N was determined using unpaired Student's *t* test. Histology and Western blot results represent at least three independent experiments.

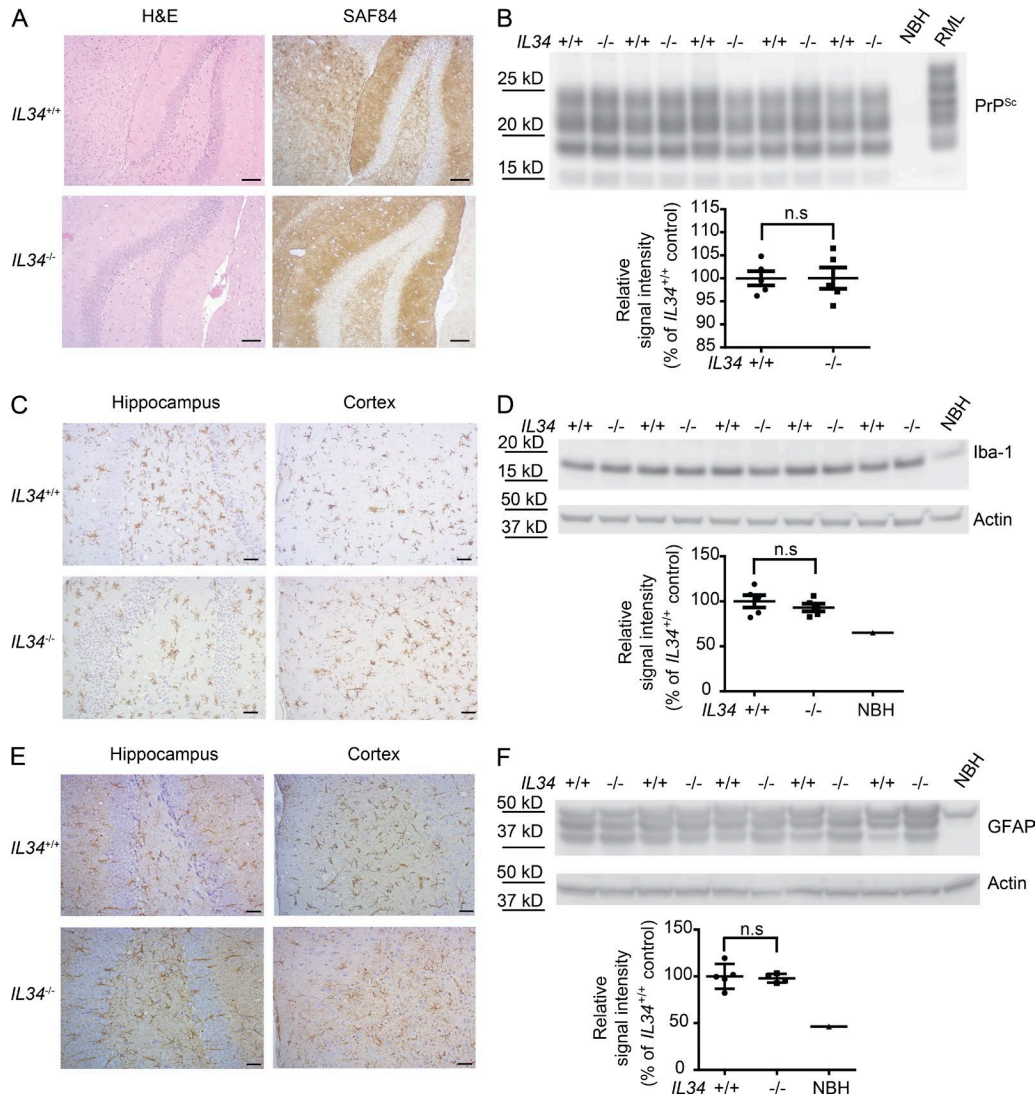


Figure 5. Similar PrP^{Sc} deposition, microglial activation, and astrogliosis in terminally sick *IL34*^{-/-} and *IL34*^{+/+} mice. (A) H&E and SAF84 immunohistochemistry of the hippocampi of terminally sick RML6-infected *IL34*^{-/-} and *IL34*^{+/+} (WT) mice. Bars, 50 μ m. (B, top) PrP^{Sc} Western blot of hemispheric brain homogenates prepared from terminally sick RML6-infected *IL34*^{-/-} and *IL34*^{+/+} (WT) mice. (bottom) Densitometric quantification of the PrP^{Sc} Western blot. *n* = 5. (C) Iba1 immunohistochemistry of hippocampi and cortex from terminally sick RML6-infected *IL34*^{-/-} and *IL34*^{+/+} (WT) mice. Bars, 20 μ m. (D, top) Iba1 Western blot of hemispheric brain homogenates prepared from terminally sick RML6-infected *IL34*^{-/-} and *IL34*^{+/+} (WT) mice. (bottom) Densitometric quantification of the Iba1 Western blot. *n* = 5. (E) GFAP immunohistochemistry of hippocampi and cortex from terminally sick RML6-infected *IL34*^{-/-} and *IL34*^{+/+} (WT) mice. Bars, 20 μ m. (F, top) GFAP Western blot of hemispheric brain homogenates prepared from terminally sick RML6-infected *IL34*^{-/-} and *IL34*^{+/+} (WT) mice. (bottom) Densitometric quantification of the GFAP Western blot. *n* = 5. Error bars represent SEM. Statistical significance in B, D, and F was determined using unpaired Student's *t* test. Histology and Western blot results represent at least five independent experiments.

influence PrP^{Sc} deposition directly in ways that were not investigated here. We favor the former interpretation because terminally sick *IL-34*^{-/-} mice and WT littermates displayed similar levels of PrP^{Sc} and a similar extent of astrogliosis.

The reduction in microglia in the *IL-34*^{-/-} system was less pronounced than in GCV-treated *tga20*/CD11b-HSV TK mice, and microglia numbers were not significantly different between prion-infected *IL-34*^{+/+} and *IL-34*^{-/-} mice at 105 and 150 dpi. This unexpected finding may be a result of

conspicuous microglia activation (and possibly proliferation) after prion infection. Nevertheless, exacerbation of prion progression was found in both models, thereby providing orthogonal lines of evidence for the protective role of microglia.

The results reported here indicate that microglia, far from mediating prion pathogenesis, are valiant defenders of the brain against prions. What might be the mechanisms by which microglia fight prion infections? The aforementioned results in concert with several previous studies converge to

indicate that phagocytosis of prion aggregates is one of the dominant lines of defense deployed by microglia. The first suggestion derived from the finding that organotypic slices devoid of microglia accumulate excessive amounts of PrP^{Sc} (Falsig et al., 2008). Here, we show that not only PrP^{Sc} accumulation is enhanced by microglial ablation, but also neurotoxicity. Second, mice lacking Milk fat globule epidermal growth factor 8 (Mfge8) experience enhanced prion accumulation and accelerated disease after prion inoculation (Kranich et al., 2010; Aguzzi et al., 2014). Mfge8 is a bifunctional secreted protein that can bind both phosphatidyl serine and integrins, thereby providing a bridge between apoptotic blebs and phagocytes. Together with the observation that prion infectivity is typically associated with lipids (Klein et al., 1998; Rouvinski et al., 2014), this finding suggests that microglia are capable of recognizing and engulfing PrP^{Sc} aggregates that expose phosphatidyl serine. The latter may derive from membrane remnants of prion-infected, dying cells.

One potential caveat of the CD11b-HSVTK microglia depletion model is that it does not differentiate microglia from infiltrating macrophages. However, the recruitment of peripheral monocytes to brain parenchyma is negligible in prion disease (Gómez-Nicola et al., 2014), and peripheral macrophages other than Langerhans cells are not affected in *IL-34*^{-/-} mice (Greter et al., 2012; Wang et al., 2012). Further studies are needed to determine whether IL-34 deficiency affects the recruitment of macrophages from the periphery to the CNS after prion infection.

A tentative conclusion derived from the present studies and previous evidence is that prionostatic strategies should avoid damage to microglia. Instead, it would be interesting to devise pharmacological tools aimed at enhancing the phagocytic capacity of microglia.

MATERIALS AND METHODS

Ethical statement. All animal experiments were performed in strict accordance with the Rules and Regulations for the Protection of Animal Rights (Tierschutzgesetz and Tier-schutzverordnung) of the Swiss Bundesamt für Lebensmittelsicherheit und Veterinärwesen and were preemptively approved by the Animal Welfare Committee of the Canton of Zürich (permit 200/2007, 90/2013, and 41/2012).

Animals. For in vivo depletion of microglia, we intercrossed *tga20*^{TK+} mice with *tga20* mice to obtain *tga20*^{+/+;Prnp^{0/0}:CD11b-HSVTK⁺ mice, henceforth referred to as *tga20*^{+/+;TK+}. To distinguish between *tga20*^{+/-} and *tga20*^{+/+} mice, we performed zygosity FISH for *Prnp*, identifying *tga20*^{+/+} founders according to published protocols (McHugh et al., 2012). For maintaining the colony, *tga20*^{+/+;TK+} females were intercrossed to *tga20* male mice as CD11b-HSVTK⁺ males are sterile (Heppner et al., 2005). *IL34*^{-/-} mice (Wang et al., 2012) carrying a targeted deletion of exons 3–5 were first backcrossed to C57BL/6J to obtain *IL34*^{+/-} offspring. *IL34*^{+/-} mice were then intercrossed to obtain *IL34*^{-/-} and *IL34*^{+/+} (WT) litter-}

mates, which were used for the experiments described here. Mice were maintained in high hygienic grade facility and housed in groups of 3–5, under a 12 h light/12 h dark cycle (from 7 a.m. to 7 p.m.) at 21 ± 1°C, with sterilized food (Kliba No. 3436; Provimi Kliba) and water ad libitum.

Organotypic slices culture preparation and microglial depletion. Cerebellar organotypic slices were prepared from 9–11-d-old pups and maintained according to previously published protocols (Falsig and Aguzzi, 2008). GCV-mediated (valganciclovir; Roche) microglia depletion experiments were performed on brain slices prepared from CD11b-HSVTK mice intercrossed with *tga20* mice (*tga20*^{TK+}). Cultures were inoculated with 100 µg brain homogenate per 10 slices from terminally sick prion-infected (RML6 and 22L) or NBH from CD1 mice, diluted in 2 ml physiological Grey's balanced salt solution (GBSS; 8 g l⁻¹ NaCl, 0.37 g l⁻¹ KCl, 0.12 g l⁻¹ Na₂HPO₄, 0.22 g l⁻¹ CaCl₂ 2H₂O, 0.09 g l⁻¹ KH₂PO₄, 0.07 g l⁻¹ MgSO₄ 7H₂O, 0.210 g l⁻¹ MgCl₂ 6H₂O, and 0.227 g l⁻¹ NaHCO₃) supplemented with the glutamate receptor antagonist kynurenic acid (1 mM; GBSSK). Slices were incubated with infectious brain homogenates as free-floating sections for 1 h at 4°C. Slices were washed twice in 6 ml GBSSK and 5–10 slices were placed on a 6-well Millicell-CM Biopore PTFE membrane insert (EMD Millipore). Residual buffer was removed and the inserts were transferred to a cell culture plate and cultured in slice culture medium (50% [vol/vol] MEM, 25% [vol/vol] basal medium Eagle, and 25% [vol/vol] horse serum supplemented with 0.65% [wt/vol] glucose, penicillin/streptomycin, and glutamax; Invitrogen). Cultures were kept in a standard cell incubator (37°C, 5% CO₂, 95% humidity), and the culture medium was exchanged three times weekly. For conditional microglia depletion, GCV (5 µg ml⁻¹) was added from 0–21 dpi reading GCV at each medium change. PLCs were obtained from 3–4-mo-old mice by peritoneal lavage using ice-cold PBS. 700,000 PLCs (counting cells with a large cell body) were added to each insert containing 10 freshly plated preinfected brain slices (70,000 PLCs/COCS). Alternatively, PLCs were sorted by MACS according to the manufacturer's (Miltenyi Biotec) protocol using antibodies raised against CD11b and CD19. Macrophages (CD19⁻, CD11b⁺) were added at 700,000 cells/insert. The purity of the sorted cell populations and the total PLCs were analyzed by flow cytometry analysis according to standard protocols using antibodies against CD3, CD19, and CD11b. Slices were harvested and analyzed for mRNA, protein or fixed for immunohistochemistry at various time points.

Intracerebral prion inoculation. Mice were intracerebrally inoculated with 30 µl of brain homogenate diluted in PBS with 5% BSA and containing 3 × 5 log LD₅₀ U of RML6. Scrapie was diagnosed according to clinical criteria (ataxia, kyphosis, priapism, and hind leg paresis). Mice were sacrificed on the day of onset of terminal clinical signs of scrapie.

Osmotic pump implantation. *Tga20^{+/+};TK⁺* and *tga20^{+/+};TK⁻* mice were intracerebrally inoculated with RML6 ($3 \times 5 \log LD_{50}$ U, 30 μ l). At 38 dpi, mice were anesthetized using isoflurane and an intraventricular catheter was implanted in the right lateral ventricle. The primed pump loaded with GCV (50 mg ml⁻¹) or PBS was placed subcutaneously and connected to the catheter. Mice received pre- and postoperative care by injection of opioids (Temgesic; 2 μ g g⁻¹ bodyweight), NSAIDs (Finadyne; 5 μ g g⁻¹ bodyweight), and glucoisotonic solution and were treated with antibiotics (Borgal; 0.1% in drinking water). Mice were kept for 2 d on a 37°C heating pad to improve surgical recovery. At terminal disease, mice were sacrificed by CO₂ inhalation, and brain, spinal cord, and cardiac blood were immediately collected. To monitor possible hematological changes, blood was analyzed by manually counting total RBCs and WBCs after lysis of RBCs. Hematocrit (the ratio of the packed blood volume over the total volume) was determined by spinning blood in heparin tubes, and then the hemoglobin concentration was determined using Drabkin's reagent (Drabkin and Austin, 1935).

Quantitative real-time PCR (qRT-PCR). Total RNA from brain or cultured slices was extracted using TRIzol (Invitrogen) according to the manufacturer's instruction. The quality of RNA was analyzed by Bioanalyzer 2100 (Agilent Technologies), RNAs with RNA integrity number >6 were used for cDNA synthesis. cDNA were synthesized from ~1 μ g total RNA using QuantiTect Reverse Transcription kit (QIAGEN) according to the manufacturer's instruction. qRT-PCR was performed using the SYBR Green PCR Master Mix (Roche) on a ViiA7 Real-Time PCR system (Applied Biosystems).

The following primer pairs were used: GAPDH sense 5'-CCACCCCAGCAAGGAGACT-3'; antisense, 5'-GAAATTGTGAGGGAGATGCT-3'. TNF sense, 5'-CATCTTCTCAAATTCGAGTGACAA-3'; antisense, 5'-TGGGAGTAGACAAGGTACAACCC-3'. IL-1 β sense, 5'-CAACCAACAAGTGATATTCTCCATG-3'; antisense, 5'-GATCCACTCTCCAGCTGCA-3'. RANTES sense, 5'-ATGCCGATTTTCCCAGGACC-3'; antisense, 5'-TTTGCCTACCTCTCCCTACTG-3'. MCP-1 sense, 5'-TTA AAAACCTGGATCGGAACCAA-3'; antisense, 5'-GCA TTAGCTTCAGATTTACGGGT-3'. IL-6 sense, 5'-TCC AATGCTCTCCTAACAGATAAG-3'; antisense, 5'-CAA GATGAATTGGATGGTCTTG-3'. Expression levels were normalized using GAPDH.

Western blot analysis. To detect PrP^{Sc} in COCS, cultures were washed twice in PBS and the tissue was scraped off the membrane using 10–15 μ l PBS per slice and homogenized by trituration using a 30-G syringe, followed by 2 \times 30-s pulses in an ultrasound bath. Protein concentration was determined using the bicinchoninic acid assay (Thermo Fisher Scientific). Samples containing the same amount of total protein were digested with PK (20 μ g protein in 20 μ l, digested with 25 μ g ml⁻¹ PK) in digestion buffer (0.5% wt/vol sodium deoxycho-

late and 0.5% vol/vol Nonidet P-40 in PBS) for 30 min at 37°C. PK digestion was stopped by adding loading buffer (NuPAGE; Invitrogen) and boiling the samples at 95°C for 5 min. Proteins were separated on a 12% Bis-Tris polyacrylamide gel (NuPAGE; Invitrogen) and blotted onto a nitrocellulose membrane. Membranes were blocked with 5% wt/vol Topblock (LuBioScience) in Tris-buffered saline supplemented with Tween (150 mM NaCl, 10 mM Tris HCl, and 0.05% vol/vol Tween 20) and incubated with POM1 mouse IgG₁ antibody to PrP^C (anti-PrP^C; 200 ng ml⁻¹) in 1% Topblock. Secondary antibodies used was horseradish peroxidase (HRP)-conjugated rabbit anti-mouse IgG₁ (1:10,000; Zymed) and the blots were developed using SuperSignal West Pico chemiluminescent substrate (Thermo Fisher Scientific) using the LAS-3000 system (FujiFilm). To detect PrP^C in the *IL34^{-/-}* and *IL34^{+/+}* (WT) brains, one hemisphere from each brain was homogenized with buffer PBS containing 0.5% Nonidet P-40 and 0.5% CHAPSO. Total protein concentration was determined using the bicinchoninic acid assay (Thermo Fisher Scientific). Approximately 8 μ g proteins were loaded and separated on a 12% Bis-Tris polyacrylamide gel (NuPAGE; Invitrogen) and then blotted onto a nitrocellulose membrane. Membranes were blocked with 5% wt/vol Topblock (LuBioScience) in PBS supplemented with 0.05% Tween 20 (vol/vol) and incubated with primary antibodies POM1 in 1% Topblock (200 ng ml⁻¹) overnight. After washing, the membranes were incubated with secondary antibody HRP-conjugated rabbit anti-mouse IgG₁ (1:10,000; Zymed). Blots were developed using Luminata Crescendo Western HRP substrate (EMD Millipore) and visualized using the Stella system (model 3200; Raytest). To avoid variation in loading, the same blots were stripped and incubated with an anti-actin antibody (1:10,000; EMD Millipore). The PrP^C signals were normalized to actin as a loading control. To detect PrP^{Sc} in prion infected *IL34^{-/-}* and *IL34^{+/+}* (WT) brains, prion-infected forebrains were homogenized in sterile 0.32 M sucrose in PBS. Total protein concentration was determined using the bicinchoninic acid assay (Thermo Fisher Scientific). Samples were adjusted to 20 μ g protein in 20 μ l and digested with 25 μ g ml⁻¹ PK in digestion buffer (PBS containing 0.5% [wt/vol] sodium deoxycholate and 0.5% [vol/vol] Nonidet P-40) for 30 min at 37°C. PK digestion was stopped by adding loading buffer (Invitrogen) and boiling samples at 95°C for 5 min. Proteins were then separated on a 12% Bis-Tris polyacrylamide gel (NuPAGE; Invitrogen) and blotted onto a nitrocellulose membrane. POM1 and HRP-conjugated rabbit anti-mouse IgG₁ were used as primary and secondary antibodies, respectively. Blots were developed using Luminata Crescendo Western HRP substrate (Millipore) and visualized using the LAS-3000 system (FujiFilm). To detect Iba-1 and GFAP in prion-infected brains by Western blot, 20 μ g of total brain protein were loaded and anti-Iba-1 antibody (1:1,000; Wako) and anti-GFAP antibody (D1F4Q) XP Rabbit mAb (1:3,000; Cell Signaling Technology) were used. Actin was used as loading control.

Immunohistochemistry. For immunohistochemistry of COCS, the organotypic slices were fixed in 4% wt/vol PFA overnight at 4°C. Membrane inserts were washed and incubated for 1 h in blocking buffer (0.05% [vol/vol] Triton X-100 and 3% vol/vol goat serum dissolved in PBS), and then incubated for 3 d at 4°C with primary antibodies diluted in blocking buffer. Slices were stained with mouse anti-Neuronal Nuclei (NeuN, 1 $\mu\text{g ml}^{-1}$; Serotec) primary antibodies and Alexa Fluor 488–conjugated secondary antibody (3 $\mu\text{g ml}^{-1}$; Molecular Probes), and then counterstained with DAPI (1 $\mu\text{g ml}^{-1}$). For quantification of NeuN immunoreactivity, images were recorded using a 4 \times lens on an Olympus BX61 fluorescence microscope equipped with a cooled black and white CCD camera. For quantification purposes all pictures were acquired at identical exposure times and the area of immunoreactivity was determined with image analysis software analySIS version 5.0, using identical grayscale threshold settings for identifying positive pixels. For quantification of microglia density, a 63 \times oil lens was used to record micrographs on a Leica SP5 confocal laser-scanning microscope.

For immunohistochemistry of prion-infected brains, formalin-fixed tissues were treated with concentrated formic acid for 60 min to inactivate prion infectivity, and then embedded in paraffin. Paraffin sections (2 μm) of brains were stained with hematoxylin and eosin (H&E). After deparaffinization through graded alcohols, antibodies GFAP (1:300; DAKO) for astrocytes were applied and visualized using standard methods, Iba-1 (1:1,000; Wako) was used for highlighting activated microglial cells. Stainings were visualized using an IVIEW DAB Detection kit (Ventana), with a hematoxylin counterstain applied subsequently. For the histological detection of partially PK-resistant prion protein deposition, deparaffinized sections were pretreated with formaldehyde for 30 min and with 98% formic acid for 6 min, and then washed in distilled water for 30 min. Sections were incubated in Ventana buffer and stains were performed on a NEXEX immunohistochemistry robot (Ventana) using an IVIEW DAB Detection kit (Ventana). After incubation with protease 1 (Ventana) for 16 min, sections were incubated with anti-PrP SAF-84 (SPI bio; A03208; 1:200) for 32 min. Sections were counterstained with hematoxylin. Sections were imaged using a Zeiss AxioPhot light microscope. Quantification of Iba-1 and GFAP staining was performed on acquired images, where regions of interest were drawn, and the percentage of brown Iba-1 and GFAP staining over the total area was quantified using in-house-developed software. The operator was blind to the genotype and treatment of the analyzed tissues.

Scoring of microglia depletion. To score microglia depletion in prion-infected CD11b–HSVTK mice, hemibrains were fixed in formalin and thin sagittal brain sections were stained for Iba1 (Wako). Brain sections were scanned at 40 \times magnification using a Hamamatsu tissue scanner (Nanozoomer), then microglia were counted automatically using the Cavalieri estimator method with a counting grid size of 34.5 \times 34.5

μm as described elsewhere (Long et al., 1998). Staining artifacts were manually excluded and ambiguous features were counted both as a positive and a negative event. Representative areas in the superior frontal cortex and central cerebellar folia were counted in two 50- μm step sections for each mouse and normalized to the result for the *tga20*^{+/+;TK+} RML6 group.

Statistical analysis. Results are presented as the mean of replicas \pm SEM. We used one-way ANOVA with Tukey's post-test for multicolumn comparison for comparison of all columns to a control column for statistical analysis of experiments involving the comparison of three or more samples. Unpaired Student's *t* test was used for comparing two samples. For in vivo experiments, all groups were compared by Log-rank (Mantel-Cox) test. P-values <0.05 were considered statistically significant.

Online supplemental material. Fig. S1 describes hematological analyses of peripheral blood in PBS or GCV-treated *tga20*/CD11b–HSVTK mice inoculated with RML or NBH. Online supplemental material is available at <http://www.jem.org/cgi/content/full/jem.20151000/DC1>.

ACKNOWLEDGMENTS

We thank the team of the Institute of Neuropathology, University Hospital Zurich, and in particular M. Delic, K. Arroyo, and M. König, for technical assistance, and M. Bieri for help with imaging and software development. We also thank Marco Colonna from Washington University School of Medicine (St. Louis, MO) for providing us with *IL34*^{-/-} mice.

A. Aguzzi is the recipient of an Advanced Grant of the European Research Council (ERC, No. 250356) and is supported by grants from the European Union (NEURIN OX), the Swiss National Foundation (including a Sinergia grant), the Swiss Initiative in Systems Biology, SystemsX.ch (PrionX, SynucleinX), the Novartis Research Foundation, the Gelu Foundation, and the Klinische Forschungsschwerpunkte ("small RNAs" and "Human Hemato-Lymphatic Diseases"). C. Zhu is the recipient of a Young Scientist Stipend of the Ernst-Jung Foundation. K. Frauenknecht is supported by a Career Development Award of the Stavros Niarchos Foundation. The funders had no role in study design, data collection and analysis, decision to publish, or preparation of the manuscript.

The authors declare no competing financial interests.

Submitted: 16 June 2015

Accepted: 5 April 2016

REFERENCES

- Aguzzi, A., and J. Falsig. 2012. Prion propagation, toxicity and degradation. *Nat. Neurosci.* 15:936–939. <http://dx.doi.org/10.1038/nn.3120>
- Aguzzi, A., B.A. Barres, and M.L. Bennett. 2013a. Microglia: scapegoat, saboteur, or something else? *Science*. 339:156–161. <http://dx.doi.org/10.1126/science.1227901>
- Aguzzi, A., M. Nuvolone, and C. Zhu. 2013b. The immunobiology of prion diseases. *Nat. Rev. Immunol.* 13:888–902. <http://dx.doi.org/10.1038/nri3553>
- Aguzzi, A., J. Kranich, and N.J. Krautler. 2014. Follicular dendritic cells: origin, phenotype, and function in health and disease. *Trends Immunol.* 35:105–113. <http://dx.doi.org/10.1016/j.it.2013.11.001>
- Alliot, F., I. Godin, and B. Pessac. 1999. Microglia derive from progenitors, originating from the yolk sac, and which proliferate in the brain. *Brain*

- Res. Dev. Brain Res.* 117:145–152. [http://dx.doi.org/10.1016/S0165-3806\(99\)00113-3](http://dx.doi.org/10.1016/S0165-3806(99)00113-3)
- Baker, C.A., D. Martin, and L. Manuelidis. 2002. Microglia from Creutzfeldt-Jakob disease-infected brains are infectious and show specific mRNA activation profiles. *J. Virol.* 76:10905–10913. <http://dx.doi.org/10.1128/JVI.76.21.10905-10913.2002>
- Brown, D.R., B. Schmidt, and H.A. Kretzschmar. 1996. Role of microglia and host prion protein in neurotoxicity of a prion protein fragment. *Nature.* 380:345–347. <http://dx.doi.org/10.1038/380345a0>
- Chen, S.K., P. Tvrđik, E. Peden, S. Cho, S. Wu, G. Spangrude, and M.R. Capecchi. 2010. Hematopoietic origin of pathological grooming in Hoxb8 mutant mice. *Cell.* 141:775–785. <http://dx.doi.org/10.1016/j.cell.2010.03.055>
- Davalos, D., J. Grutzendler, G. Yang, J.V. Kim, Y. Zuo, S. Jung, D.R. Littman, M.L. Dustin, and W.B. Gan. 2005. ATP mediates rapid microglial response to local brain injury in vivo. *Nat. Neurosci.* 8:752–758. <http://dx.doi.org/10.1038/nm1472>
- Derecki, N.C., J.C. Cronk, Z. Lu, E. Xu, S.B. Abbott, P.G. Guyenet, and J. Kipnis. 2012. Wild-type microglia arrest pathology in a mouse model of Rett syndrome. *Nature.* 484:105–109. <http://dx.doi.org/10.1038/nature10907>
- Drabkin, D.L., and J.H. Austin. 1935. Preparations from washed blood cells; nitric oxide hemoglobin and sulfhemoglobin. *J. Biol. Chem.* 112:51–65.
- Falsig, J., and A. Aguzzi. 2008. The prion organotypic slice culture assay—POS CA. *Nat. Protoc.* 3:555–562. <http://dx.doi.org/10.1038/nprot.2008.13>
- Falsig, J., C. Julius, I. Margalith, P. Schwarz, F.L. Heppner, and A. Aguzzi. 2008. A versatile prion replication assay in organotypic brain slices. *Nat. Neurosci.* 11:109–117. <http://dx.doi.org/10.1038/nm2028>
- Falsig, J., T. Sonati, U.S. Herrmann, D. Saban, B. Li, K. Arroyo, B. Ballmer, P.P. Liberski, and A. Aguzzi. 2012. Prion pathogenesis is faithfully reproduced in cerebellar organotypic slice cultures. *PLoS Pathog.* 8:e1002985. <http://dx.doi.org/10.1371/journal.ppat.1002985>
- Fischer, M., T. Rüllicke, A. Raeber, A. Sailer, M. Moser, B. Oesch, S. Brandner, A. Aguzzi, and C. Weissmann. 1996. Prion protein (PrP) with amino-proximal deletions restoring susceptibility of PrP knockout mice to scrapie. *EMBO J.* 15:1255–1264.
- Giese, A., D.R. Brown, M.H. Groschup, C. Feldmann, I. Haist, and H.A. Kretzschmar. 1998. Role of microglia in neuronal cell death in prion disease. *Brain Pathol.* 8:449–457. <http://dx.doi.org/10.1111/j.1750-3639.1998.tb00167.x>
- Ginhoux, F., M. Greter, M. Leboeuf, S. Nandi, P. See, S. Gokhan, M.F. Mehler, S.J. Conway, L.G. Ng, E.R. Stanley, et al. 2010. Fate mapping analysis reveals that adult microglia derive from primitive macrophages. *Science.* 330:841–845. <http://dx.doi.org/10.1126/science.1194637>
- Gómez-Nicola, D., N.L. Fransen, S. Suzzi, and V.H. Perry. 2013. Regulation of microglial proliferation during chronic neurodegeneration. *J. Neurosci.* 33:2481–2493. <http://dx.doi.org/10.1523/JNEUROSCI.4440-12.2013>
- Gómez-Nicola, D., S.T. Schettlers, and V.H. Perry. 2014. Differential role of CCR2 in the dynamics of microglia and perivascular macrophages during prion disease. *Glia.* 62:1041–1052. <http://dx.doi.org/10.1002/glia.22660>
- Grathwohl, S.A., R.E. Kälin, T. Bolmont, S. Prokop, G. Winkelmann, S.A. Kaeser, J. Odenthal, R. Rädde, T. Eldh, S. Gandy, et al. 2009. Formation and maintenance of Alzheimer's disease β -amyloid plaques in the absence of microglia. *Nat. Neurosci.* 12:1361–1363. <http://dx.doi.org/10.1038/nn.2432>
- Greter, M., I. Lelios, P. Pelczar, G. Hoeffel, J. Price, M. Leboeuf, T.M. Kündig, K. Frei, F. Ginhoux, M. Merad, and B. Becher. 2012. Stroma-derived interleukin-34 controls the development and maintenance of langerhans cells and the maintenance of microglia. *Immunity.* 37:1050–1060. <http://dx.doi.org/10.1016/j.immuni.2012.11.001>
- Hanisch, U.K., and H. Kettenmann. 2007. Microglia: active sensor and versatile effector cells in the normal and pathologic brain. *Nat. Neurosci.* 10:1387–1394. <http://dx.doi.org/10.1038/nn1997>
- Heppner, F.L., M. Greter, D. Marino, J. Falsig, G. Raivich, N. Hövelmeyer, A. Waisman, T. Rüllicke, M. Prinz, J. Priller, et al. 2005. Experimental autoimmune encephalomyelitis repressed by microglial paralysis. *Nat. Med.* 11:146–152. <http://dx.doi.org/10.1038/nm1177>
- Herrmann, U.S., T. Sonati, J. Falsig, R.R. Reimann, P. Dametto, T. O'Connor, B. Li, A. Lau, S. Hornemann, S. Sorce, et al. 2015. Prion infections and anti-PrP antibodies trigger converging neurotoxic pathways. *PLoS Pathog.* 11:e1004662. <http://dx.doi.org/10.1371/journal.ppat.1004662>
- Hughes, M.M., R.H. Field, V.H. Perry, C.L. Murray, and C. Cunningham. 2010. Microglia in the degenerating brain are capable of phagocytosis of beads and of apoptotic cells, but do not efficiently remove PrPSc, even upon LPS stimulation. *Glia.* 58:2017–2030. <http://dx.doi.org/10.1002/glia.21070>
- Jeffrey, M., C.M. Goodsir, M.E. Bruce, P.A. McBride, and C. Farquhar. 1994. Morphogenesis of amyloid plaques in 87V murine scrapie. *Neuropathol. Appl. Neurobiol.* 20:535–542. <http://dx.doi.org/10.1111/j.1365-2990.1994.tb01007.x>
- Kierdorf, K., D. Erny, T. Goldmann, V. Sander, C. Schulz, E.G. Perdiguerro, P. Wieghofer, A. Heinrich, P. Riemke, C. Hölscher, et al. 2013. Microglia emerge from erythromyeloid precursors via Pu.1- and Irf8-dependent pathways. *Nat. Neurosci.* 16:273–280. <http://dx.doi.org/10.1038/nn.3318>
- Klein, T.R., D. Kirsch, R. Kaufmann, and D. Riesner. 1998. Prion rods contain small amounts of two host sphingolipids as revealed by thin-layer chromatography and mass spectrometry. *Biol. Chem.* 379:655–666. <http://dx.doi.org/10.1515/bchm.1998.379.6.655>
- Kranich, J., N.J. Krautler, J. Falsig, B. Ballmer, S. Li, G. Hutter, P. Schwarz, R. Moos, C. Julius, G. Miele, and A. Aguzzi. 2010. Engulfment of cerebral apoptotic bodies controls the course of prion disease in a mouse strain-dependent manner. *J. Exp. Med.* 207:2271–2281. <http://dx.doi.org/10.1084/jem.20092401>
- Long, J.M., A.N. Kalehua, N.J. Muth, J.M. Hengemihle, M. Jucker, M.E. Calhoun, D.K. Ingram, and P.R. Mouton. 1998. Stereological estimation of total microglia number in mouse hippocampus. *J. Neurosci. Methods.* 84:101–108. [http://dx.doi.org/10.1016/S0165-0270\(98\)00100-9](http://dx.doi.org/10.1016/S0165-0270(98)00100-9)
- McHugh, D., T. O'Connor, J. Bremer, and A. Aguzzi. 2012. ZyFISH: a simple, rapid and reliable zygosity assay for transgenic mice. *PLoS One.* 7:e37881. <http://dx.doi.org/10.1371/journal.pone.0037881>
- Mildner, A., B. Schlevogt, K. Kierdorf, C. Böttcher, D. Erny, M.P. Kummer, M. Quinn, W. Brück, I. Bechmann, M.T. Heneka, et al. 2011. Distinct and non-redundant roles of microglia and myeloid subsets in mouse models of Alzheimer's disease. *J. Neurosci.* 31:11159–11171. <http://dx.doi.org/10.1523/JNEUROSCI.6209-10.2011>
- Nimmerjahn, A., F. Kirchhoff, and F. Helmchen. 2005. Resting microglial cells are highly dynamic surveillants of brain parenchyma in vivo. *Science.* 308:1314–1318. <http://dx.doi.org/10.1126/science.1110647>
- Paolicelli, R.C., G. Bolasco, F. Pagani, L. Maggi, M. Scianni, P. Panzanelli, M. Giustetto, T.A. Ferreira, E. Guiducci, L. Dumas, et al. 2011. Synaptic pruning by microglia is necessary for normal brain development. *Science.* 333:1456–1458. <http://dx.doi.org/10.1126/science.1202529>
- Parkhurst, C.N., G. Yang, I. Ninan, J.N. Savas, J.R. Yates III, J.J. Lafaille, B.L. Hempstead, D.R. Littman, and W.B. Gan. 2013. Microglia promote learning-dependent synapse formation through brain-derived neurotrophic factor. *Cell.* 155:1596–1609. <http://dx.doi.org/10.1016/j.cell.2013.11.030>
- Rogers, J.T., J.M. Morganti, A.D. Bachstetter, C.E. Hudson, M.M. Peters, B.A. Grimmig, E.J. Weeber, P.C. Bickford, and C. Gemma. 2011. CX3CR1 deficiency leads to impairment of hippocampal cognitive function and

- synaptic plasticity. *J. Neurosci.* 31:16241–16250. <http://dx.doi.org/10.1523/JNEUROSCI.3667-11.2011>
- Rouvinski, A., S. Karniely, M. Kounin, S. Moussa, M.D. Goldberg, G. Warburg, R. Lyakhovetsky, D. Papy-Garcia, J. Kutzsche, C. Korth, et al. 2014. Live imaging of prions reveals nascent PrP^{Sc} in cell-surface, raft-associated amyloid strings and webs. *J. Cell Biol.* 204:423–441. <http://dx.doi.org/10.1083/jcb.201308028>
- Schafer, D.P., E.K. Lehrman, A.G. Kautzman, R. Koyama, A.R. Mardinly, R. Yamasaki, R.M. Ransohoff, M.E. Greenberg, B.A. Barres, and B. Stevens. 2012. Microglia sculpt postnatal neural circuits in an activity and complement-dependent manner. *Neuron.* 74:691–705. <http://dx.doi.org/10.1016/j.neuron.2012.03.026>
- Schulz, C., E. Gomez Perdiguero, L. Chorro, H. Szabo-Rogers, N. Cagnard, K. Kierdorf, M. Prinz, B. Wu, S.E. Jacobsen, J.W. Pollard, et al. 2012. A lineage of myeloid cells independent of Myb and hematopoietic stem cells. *Science.* 336:86–90. <http://dx.doi.org/10.1126/science.1219179>
- Sonati, T., R.R. Reimann, J. Falsig, P.K. Baral, T. O'Connor, S. Hornemann, S. Yaganoglu, B. Li, U.S. Herrmann, B. Wieland, et al. 2013. The toxicity of anti-prion antibodies is mediated by the flexible tail of the prion protein. *Nature.* 501:102–106. <http://dx.doi.org/10.1038/nature12402>
- Wang, Y., K.J. Szretter, W. Vermi, S. Gilfillan, C. Rossini, M. Cella, A.D. Barrow, M.S. Diamond, and M. Colonna. 2012. IL-34 is a tissue-restricted ligand of CSF1R required for the development of Langerhans cells and microglia. *Nat. Immunol.* 13:753–760. <http://dx.doi.org/10.1038/ni.2360>
- Williams, A., P.J. Lucassen, D. Ritchie, and M. Bruce. 1997. PrP deposition, microglial activation, and neuronal apoptosis in murine scrapie. *Exp. Neurol.* 144:433–438. <http://dx.doi.org/10.1006/exnr.1997.6424>
- Zhan, Y., R.C. Paolicelli, F. Sforzini, L. Weinhard, G. Bolasco, F. Pagani, A.L. Vyssotski, A. Bifone, A. Gozzi, D. Ragozzino, and C.T. Gross. 2014. Deficient neuron-microglia signaling results in impaired functional brain connectivity and social behavior. *Nat. Neurosci.* 17:400–406. <http://dx.doi.org/10.1038/nn.3641>